Langmuir

Article

pubs.acs.org/Langmuir

Real-Time Observation of the Swelling and Hydrolysis of a Single Crystalline Cellulose Fiber Catalyzed by Cellulase 7B from *Trichoderma reesei*

Jingpeng Wang,[†] Amanda Quirk,[†] Jacek Lipkowski,*[,†] John R. Dutcher,[‡] Christopher Hill,[∥] Adam Mark,[§] and Anthony J. Clarke[§]

[†]Department of Chemistry, [‡]Department of Physics, and [§]Department of Molecular and Cellular Biology, University of Guelph, Guelph, Ontario N1G 2W1, Canada

[∥]Iogen Corporation, 310 Hunt Club Road East, Ottawa, Ontario K1V 1C1, Canada

Supporting Information

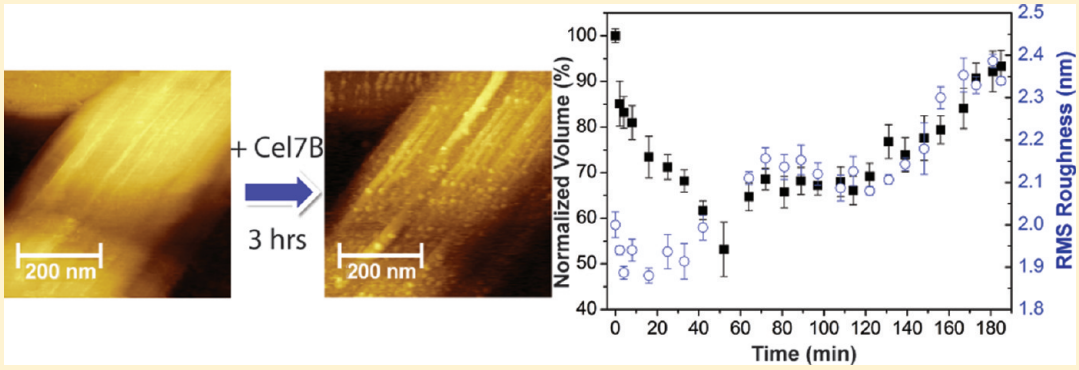

ABSTRACT: The biodegradation of cellulose involves the enzymatic action of cellulases (endoglucanases), cellobiohydrolases (exoglucanases), and β-glucosidases that act synergistically. The rate and efficiency of enzymatic hydrolysis of crystalline cellulose in vitro decline markedly with time, limiting the large-scale, cost-effective production of cellulosic biofuels. Several factors have been suggested to contribute to this phenomenon, but there is considerable disagreement regarding the relative importance of each. These earlier investigations were hampered by the inability to observe the disruption of crystalline cellulose and its subsequent hydrolysis directly. Here, we show the application of high-resolution atomic force microscopy to observe the swelling of a single crystalline cellulose fiber and its-hydrolysis in real time directly as catalyzed by a single cellulase, the industrially important cellulase 7B from *Trichoderma reesei*. Volume changes, the root-mean-square roughness, and rates of hydrolysis of the surfaces of single fibers were determined directly from the images acquired over time. Hydrolysis dominated the early stage of the experiment, and swelling dominated the later stage. The high-resolution images revealed that the combined action of initial hydrolysis followed by swelling exposed individual microfibrils and bundles of microfibrils, resulting in the loosening of the fiber structure and the exposure of microfibrils at the fiber surface. Both the hydrolysis and swelling were catalyzed by the native cellulase; under the same conditions, its isolated carbohydrate-binding module did not cause changes to crystalline cellulose. We anticipate that the application of our AFM-based analysis on other cellulolytic enzymes, alone and in combination, will provide significant insight into the process of cellulose biodegradation and greatly facilitate its application for the efficient and economical production of cellulosic ethanol.

INTRODUCTION

Cellulose is the earth's most abundant biopolymer, constituting about one-half of the carbon in the biosphere, and thus it represents a major potential feedstock for producing sustainable biofuels. It is an unbranched homopolymer of D-glucose units linked together by β-(1,4)-glycosidic bonds to form chains extending 300 to 10 000 units in length, depending on its source. Despite this compositional simplicity, both the physical structure and morphology of native cellulose are complex and heterogeneous.[1] It has hierarchical structure that consists of individual glucan chains with a cross section of ~1 nm that stack and adhere to each other by means of intra- and intermolecular hydrogen-bonding networks and van der Waals forces to form structurally rigid crystalline microfibrils[2] with cross sections on the order of 4−6 nm. These microfibrils are the building blocks of macrofibrils with cross sections of 10−100 nm, and the stacking of macrofibrils gives fibrils with cross sections in the range of 0.1−1 μm for two distinct

Received: March 13, 2012
Revised: May 22, 2012
Published: May 30, 2012

allomorphs, cellulose Iα and Iβ.[3,4] The complexity and rigidity of cellulose make it ideal for its role as the major structural component of plant cell walls but poses significant challenges for its efficient conversion to glucose for the production of biofuel. Many biofuel processes convert cellulose to glucose using enzymatic hydrolysis.

The biodegradation of cellulose into glucose involves the concerted action of three different enzymes of microbial origin (both bacterial and fungal): cellulases, cellobiohydrolases, and β-glucosidases.[1] Cellulases (E.C. 3.2.1.4, endoglucanase) are endo-acting enzymes that attack glycosidic bonds randomly within cellulose chains to create new chain ends for cellobiohydrolase action and the release of soluble cello-oligosaccharides. As exo-enzymes, cellobiohydrolases (E.C. 3.2.1.91, exoglucanases) release cellobiose units from the chain ends of either insoluble cellulose or cello-oligosaccharides. The β-glucosidases (E.C. 3.2.1.21) complete the hydrolytic process by cleaving the cellobiose and short-chain cello-oligosaccharides into their constituent glucose units. Many of these cellulolytic enzymes have a multimodular organization that typically involves combinations of catalytic domains that are responsible for catalyzing the hydrolysis and carbohydrate-binding modules (CBM) that are responsible for adsorption to the crystalline regions of cellulose.

The complementarity of the endo- and exo-activities of the cellulases and cellobiohydrolases results in synergism[5] that produces very efficient biodegradation of natural cellulose. However, the scale up of this process to industrial levels for biofuel production has proven to be extremely challenging, with ready access and binding of the cellulolytic enzymes to their appropriate sites of action being the primary limiting factors. In addition, the rate and efficiency of enzymatic hydrolysis in vitro decline markedly with time, thereby exacerbating the inefficiency of the large-scale production of cellulosic biofuels.[6,7] The properties of both the cellulosic substrate and the cellulolytic enzymes may contribute to this phenomenon. In nature, plant cellulose is associated with other cell wall polymers, such as lignin, xylan, and arabinogalactan, and its crystallinity, degree of polymerization, and accessible surface area vary greatly. For the enzymes, effects such as end-product inhibition, the need for synergism, and irreversible enzyme adsorption or inactivation can contribute to the rate reduction.[8−11] However, there remains considerable disagreement regarding the relative importance of each of these factors. Earlier studies investigating these issues were hampered by the inability to observe the disruption of crystalline cellulose and its subsequent hydrolysis directly. The recent application of high-resolution atomic force microscopy (AFM), however, has provided some insight into these underlying causes.

AFM offers the opportunity to observe the enzymatic degradation of crystalline cellulose fibers directly on the nanometer scale. It has been used to study the crystal structure and microfibril surface and assembly of cellulose[12−14] and to probe the mechanism of cellulose−enzyme interactions.[15−19] Most of the latter studies have concerned cellobiohydrolases, which were previously thought to be responsible for the swelling of cellulose, in addition to their hydrolytic activity. Thus, cellobiohydrolase I (CBHI, Cel7A) from *Trichoderma reesei* has been observed to cause morphological changes to bacterial cellulose (BC),[15] and real-time AFM images have been interpreted in terms of the selective hydrolysis by this exocellulase of the hydrophobic faces of cellulose.[16] Igarashi et al. subsequently demonstrated the progressive movement of this CBHI on crystalline cellulose,[17] and more recently, they captured in real time the intermittent repeat stop and start movements of the enzyme along the surface of crystalline cellulose.[18] In contrast to the several AFM studies in which the effect of CBHs has been investigated, there have been very few microscopy studies on the action of cellulases on natural crystalline cellulose fibers.

Recently, we reported in situ AFM imaging of the enzymatic hydrolysis of never-dried, single BC fibers by cellulase A (CenA) from the bacterium *Cellulomonas fimi*.[19] This study provided the first real-time images of the enzymatic degradation of a single cellulose fiber on the nanometer scale. We have since extended these studies to include the action of the major cellulase of *T. reesei*, cellulase 7B (Cel7B, also known as endoglucanase I (EGI)). This cellulase, which accounts for 5−10% of the total amount of the cellulolytic enzymes produced by this industrially important fungus, has a molecular mass of ∼50 kDa, and its crystal structure has been well characterized.[20,21] Many earlier studies indicated that it exhibits a high level of hydrolytic activity on amorphous cellulose and soluble cellulose derivatives but it hydrolyzes crystalline cellulose at a significantly slower rate.[5,22]

In the present study, we have performed in situ AFM imaging of Cel7B activity on a single native bacterial cellulose fiber in aqueous buffer for the identification of the specific fiber regions targeted by the enzyme. In addition to visualizing hydrolytic activity in real time, we provide the first direct visualization of the topographic changes caused by Cel7B, which includes the swelling of the crystalline microfibrils. We provide unique information on the effect of the enzyme on the hierarchical structure of the fiber. Specifically, we demonstrated that Cel7B enzyme loosens the hierarchical structure of the crystalline cellulose and exposes single microfibrils. This is significant information that explains the synergistic role of Cel7B in a mixture with Cel7A and Cel6A enzymes.

EXPERIMENTAL SECTION

Materials. To minimize contamination, self-assembled monolayers (SAM) of 1-thio-D-glucose (TG) on a gold substrate were freshly prepared before use in AFM studies from 2 mM thiol solutions of 1-thio-D-glucose (Sigma) in spectroscopic-grade methanol (99.96%, Fisher Scientific). The gold substrate used in all AFM experiments consisted of a 200-nm-thick gold film evaporated onto a clean glass slide that was pretreated by the deposition of a 2-nm-thick layer of chromium to ensure better adhesion. The gold slide was annealed in a muffle furnace at 675 °C for a period of 60 s prior to each SAM modification process. Unless otherwise indicated, the electrolyte for all AFM imaging experiments was 50 mM citrate buffer (pH 5.0), prepared from sodium citrate (99.9%, Alfa Aesar) and anhydrous citric acid (99.5%, Fluka). Millipore ultrapure water (resistivity 18.2 MΩ cm at 25 °C) was used for all aqueous solutions.

Preparation of Cellulose Fiber Thin Films. Bacterial cellulose (BC) is preferred over plant cellulose for AFM studies because it is obtained in higher purity (i.e., no contaminating hemicellulose or lignin) and it exhibits both a higher degree of polymerization and a higher crystallinity index. Native BC fibers were obtained from *Acetobacter xylinum*,[23] and they were prepared for thin films as described by Quirk et al.[19] The immobilization of cellulose thin films onto a TG-modified gold substrate was performed using the Langmuir−Blodgett (LB) technique in which floating BC fibers can be reproducibly transferred onto the substrate, resulting in a thin layer consisting of a large number of isolated single fibers.[19] The freshly prepared cellulose fibers were used immediately in AFM imaging experiments.

Purification of *T. reesei* Cel7B. The cellulase was isolated and purified from a commercial preparation of the *T. reesei* enzyme secretome (Iogen Corporation). It was purified from the crude filtrate by anion-exchange chromatography on DEAE-Sepharose as described by Bhikhabhai et al.[24] Ultrafiltration was used both to concentrate the

dx.doi.org/10.1021/la301030f | *Langmuir* 2012, 28, 9664−9672

purified Cel7B and to exchange the buffer with 50 mM sodium citrate (pH 5.0) prior to dividing into aliquots and storing at −20 °C. Stock enzyme solutions used for each AFM imaging experiment were prepared by thawing one aliquot of Cel7B in 10 mL of a 50 mM citrate buffer (pH 5.0).

Protein concentrations were determined using the method of Bradford et al.[25] SDS-PAGE was performed using the method of Laemmli[26] with Commassie Blue staining. The staining intensity of each band was quantified by scanning densitometry using a Chemigenius2 (Syngene) imaging system. To ensure that these preparations were devoid of other contaminating cellulolytic enzymes, samples were analyzed by Western immunoblotting using component-specific polyclonal antisera from rabbit (data not shown).[27] The component-specific polyclonal antisera were generated using synthetic peptides, the sequences of which were based on the primary amino acid sequence of Cel7B from *T. reesei*. The purity was in excess of 90% as judged by SDS-PAGE stained with Coomassie Blue and a Western blot. (Detailed purity data are shown in Figure SI 1 of the Supporting Information.) SDS-PAGE revealed a strong band and a second small, faint band. Western blot analysis using anti-Cel7B showed only a band in the Cel7B lane. None of seven major cellulose-active enzymes (Cel7A, Cel6A, Cel5A, Cel61A, Swo1, or Cip1) were present in the Cel7B preparation. The small, faint band, which is present in very low abundance, likely makes no or a negligible contribution to the cellulose hydrolysis.

Expression and Purification of the GFP-CBM Construct. A synthetic gene encoding a chimeric protein (Figure 1) comprising an N-terminal hexa-histidine tag, a truncated linker domain, and family 1 CBM from *T. reesei* Cel7B was constructed in a pET-30b(+) vector (EMD Biosciences). Its lactose-inducible promoter was used for the intracellular expression of the construct in transformed cells of *Escherichia coli* BL21-CodonPlus(D3) (Stratagene). Briefly, an overnight culture was grown in SOC media at 37 °C and used to inoculate shake flasks containing 250 mL of SOC. The inoculated flasks were incubated at 37 °C with orbital shaking until the optical densities of the cultures reached 0.6. Expression was then induced with the addition of 1 mL of 100 mM isopropyl β-D-1-thiogalactopyranoside to each 250 mL culture. The temperature was reduced to 30 °C, and expression was allowed to proceed for 3 h. The cell mass was recovered by centrifugation, frozen at −20 °C, and lysed using BugBuster (EMD Biosciences) reagent.

HHHHHHSGLVPRGSGMKETAAAKFERQHM
DSPDLGTDDDDKAMAISDPNSSSVDKLM−
KGEELFTGVVPILVELDGDVNNGHKFSVS
GEGEGDATYGKLTLKFICTTGKLPVPWPT
LVTTLCYGVQCFSRYPDHMKRHDFFKSAM
PEGYVQERTIFFKDDGNYKTRAEVKFEGD
TLVNRIELKGIDFKEDGNILGHKLEYNYN
SHNVYIMADKQKNGIKVNFKTRHNIEDGS
VQLADHYQQNTPIGDGPVLLPDNHYLSTQ
SALSKDPNEKRDHMVLLEFVTAAGITHGM
DELYNGSTTSSSPSCTQTHWGQCGGIGYS
GCKTCTSGTTCQYSNDYYSQCL

Figure 1. Amino acid sequence of the GFP-CBM fusion protein. The N-terminal hexa-histidine tag (orange) is followed sequentially by a linker sequence (gray), the green fluorescent protein (green), a second linker (gray), and type 1 CBM from *T. reesei* Cel7B (yellow).

Cell mass lysates were clarified by filtration using a Stericup (Millipore), diluted in binding buffer, and filtered again with a glass-fiber filter. The fusion protein was purified from these lysates using immobilized-metal affinity chromatography. Briefly, samples of the lysates were added to 5 mL HisTrap HP columns (GE Healthcare) previously equilibrated with binding buffer (200 mM NaCl, 20 mM NaH_2PO_4, 30 mM imidazole, pH 7.4). The columns were washed with additional binding buffer until a stable UV_{280} reading was reached and the GFP-CBM bound to the column via its hexa-histidine tag was eluted with an elution buffer (20 mM NaH_2PO_4, 500 mM imidazole, pH 7.4). Fractions containing the CBM were pooled, and a spin concentrator was used to exchange the protein in 10 mM Tris at pH 8.0. The purified and concentrated GFP-CBM was divided into aliquots and stored at −20 °C. Prior to each AFM imaging experiment, one frozen aliquot of GFP-CBM was added to a 10 mM phosphate buffer at pH 8.0 to provide a stock solution. The enzyme activity toward cellulose fiber hydrolysis was tested using the reducing sugar assay. The results of these tests are shown in Figures SI-2 and SI-3 of the Supporting Information.

AFM Imaging and Data Analysis. AFM images were collected using a Pico SPM Microscope (Molecular Imaging) with an AFMS 182 scanner and the PicoScan 5.3 software system. All imaging experiments were operated in magnetic ac (MAC) mode using tip B of type I MAClevers (Agilent Technologies). The average thickness, width, length, and nominal force constant of this cantilever were approximately 1.0 μm, 35 μm, 90 μm, and 1.75 N/m, respectively. The feedback loop was adjusted to 20−25% amplitude reduction (i.e., the amplitude set point) to maintain the tip−sample interaction in the light tapping regime. A homemade AFM liquid cell was equipped with capillary ports for the addition of enzyme solutions for in situ imaging experiments. All imaging trials were carried out in 50 mM citrate buffer (pH 5.0) at room temperature (20 ± 2 °C). To ensure absolute stability, the AFM was located in a specially designed laboratory with an acoustic and vibration isolation cage.

Changes in cellulose surface structure during an ongoing hydrolysis reaction were monitored by continuous time-lapse AFM imaging. In every trial, a single cellulose fiber was chosen as the imaging target and was monitored for at least 30 min prior to adding enzyme to ensure that the system (temperature, mechanical drift, noise level, and firmness of fiber−substrate attachment) was stable. Then, a precise amount of enzyme stock solution was injected very carefully such that the original target fiber was not disturbed. In general, each real-time AFM image of the same target fiber was obtained repetitively at a scan speed of 2 to 3 Hz, which resulted in a total recording time of ca.

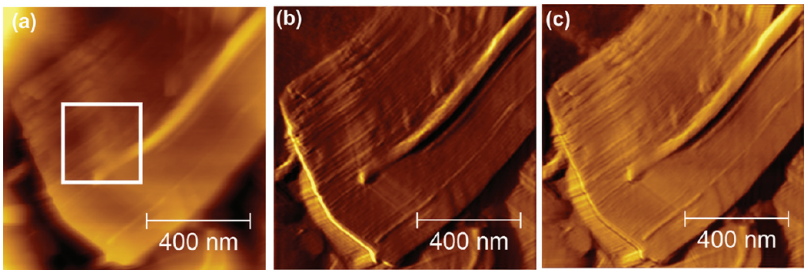

Figure 2. AFM images of crystalline bacterial cellulose in 50 mM citrate buffer at pH 5.0 on thioglucose-modified gold. The images were obtained in MAC mode from channels of (a) topography, (b) amplitude, and (c) phase.

dx.doi.org/10.1021/la301030f | *Langmuir* 2012, 28, 9664−9672

2 min per image and up to 3 to 4 h under the incubation of enzyme in buffer solution. A movie that was constructed by connecting a series of time-lapse AFM topography images is available in the Supporting Information. The time interval between each image frame was 0.5 s. Image drift was corrected by cropping to the center region of each image.

Data analysis, including cross-section and roughness measurements, and volume calculations were performed only on AFM topography images using Gwyddion v2.26 software. Each topography image was processed with a second-order polynomial background leveling with all of the fiber regions excluded. Lines that were used to measure cross sections of fiber surfaces were always drawn using line widths of a few pixels to extract average information. The volume of a selected fiber segment was determined by using the grain analysis function in Gwyddion: a mask on surface grains was first applied via the height threshold control, and then the volume was obtained using the grain minimum basis algorithm. On the basis of multiple careful attempts to measure selected fiber volumes and roughnesses from each image, we found that maximum errors of ±3% and ±5% were associated with the surface rms roughness and volume measurements, respectively.

Tip artifacts are an ever-present problem in AFM imaging studies. Several precautions were taken to minimize this problem. First, an AFM tip calibration kit containing colloidal gold particles (5, 10, 15, 20, and 30 nm diameter, Pelco standard kit 16205, Ted Pella, Inc.) was used to characterize the tips used in this work. Second, new tips were always used for every trial. Third, at the beginning of each trial the scan direction was always rotated by 45 and 90° while keeping all other settings the same to ensure that the obtained images had minimal tip artifacts. Because the dimensions of the imaged microfibrils were comparable to that of the AFM probe used, many of the features observed in the AFM images were convoluted with the tip geometry, and the result was a broadening of the lateral dimensions in the topographical image of the microfibrils.[28] Therefore, a tip-deconvolution procedure was performed to minimize this effect.[19] In this work, all of the topography images used in the quantitative analysis were corrected for any tip-broadening effect by employing a tip-deconvolution module (using blind estimation and a surface-reconstruction method) in the commercial SPIP software package (ImageMetrology Ltd., Denmark). Scanning electron microscopy (SEM) was used as previously described[19] to determine the true tip geometry instead of using the nominal specifications of the tip geometry provided by the manufacturer. In the SEM images, the AFM tip used for imaging was observed to have a conical shape with a radius of apex curvature that was determined to be 15 ± 5 nm.

The most prevalent complication in AFM imaging is image drift, which makes the tracking of a single cellulose fiber difficult and impedes the collection of quantitative data. One of the major contributing factors is the thermal drift in the piezoelectric scanner as a result of changes in temperature. We attempted to minimize the drift by allowing the AFM setup with the attached liquid cell to equilibrate for 1 to 3 h before the enzyme experiments were performed. This significantly decreased the drift, but it did not eliminate it entirely.

RESULTS AND DISCUSSION

Control Experiments. In a typical MAC-mode AFM experiment, three types of images can be obtained simultaneously: topography (Figure 2a), amplitude (Figure 2b), and phase (Figure 2c). Topography images contain information about the physical dimensions of the fiber. The fiber shown in Figure 2a is ca. 600 nm wide and ca. 5−10 nm in height. It has a flat ribbon shape characteristic of cellulose fibers from bacterial sources.[29] The amplitude image is generated as the error signal between the set point and the real detector signal, thus emphasizing changes in elevation. Because it is equivalent to a map of the slope of surface features on the sample, the amplitude image often enhances the edges of surface features that may not be easily distinguished in topography images.[30] The microfibrils seen on the fiber surface have an improved contrast in Figure 2b. The phase image originates from the phase lag of the cantilever oscillations relative to the drive signal caused by differences in adhesive forces, stiffness, and/or viscoelastic properties. The contrast in the phase image is a powerful tool for differentiating materials/boundaries with high or low tip−substrate interactions.[31] In Figure 2c, the phase contrast provides the best distinction of the fiber from the background of the substrate surface. By combining the three image channels, a better understanding of the sample is obtained. In this work, quantitative analysis of the enzyme-induced changes in the fiber morphology was performed on the

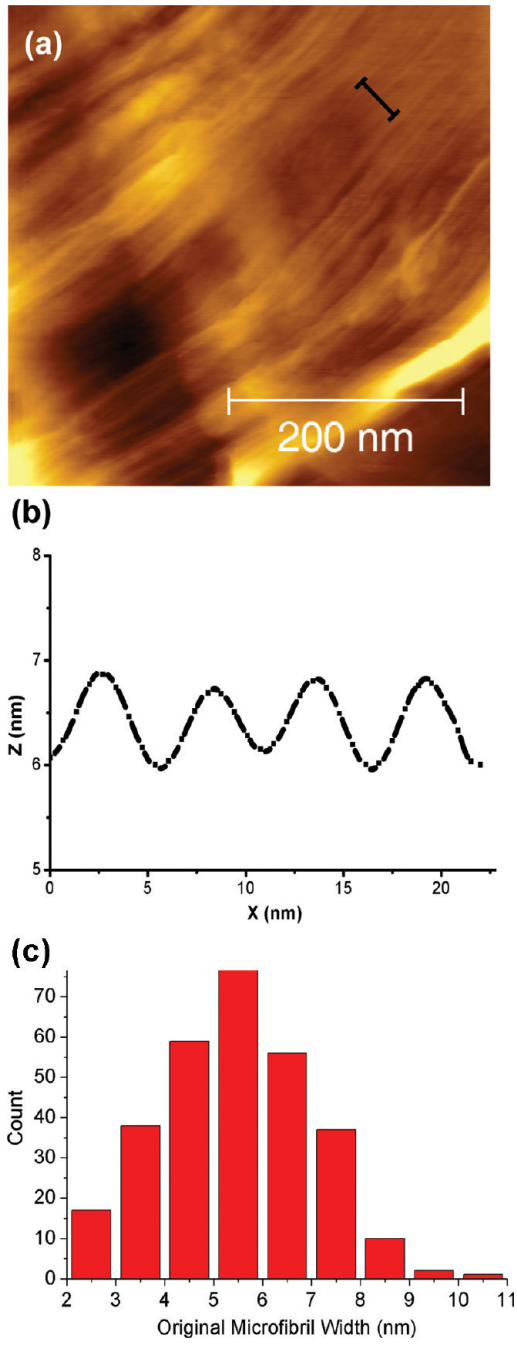

Figure 3. Determination of physical dimensions of crystalline cellulose by high-resolution AFM. (a) High-resolution topography image corresponding to the area within the white box of Figure 2a. (b) Height profile corresponding to the image under the cross-sectional line in part a, with a line width of 10 nm and the baseline corrected. (c) Distribution of widths of 300 different microfibrils (average width = 5 ± 2 nm).

dx.doi.org/10.1021/la301030f | Langmuir 2012, 28, 9664−9672

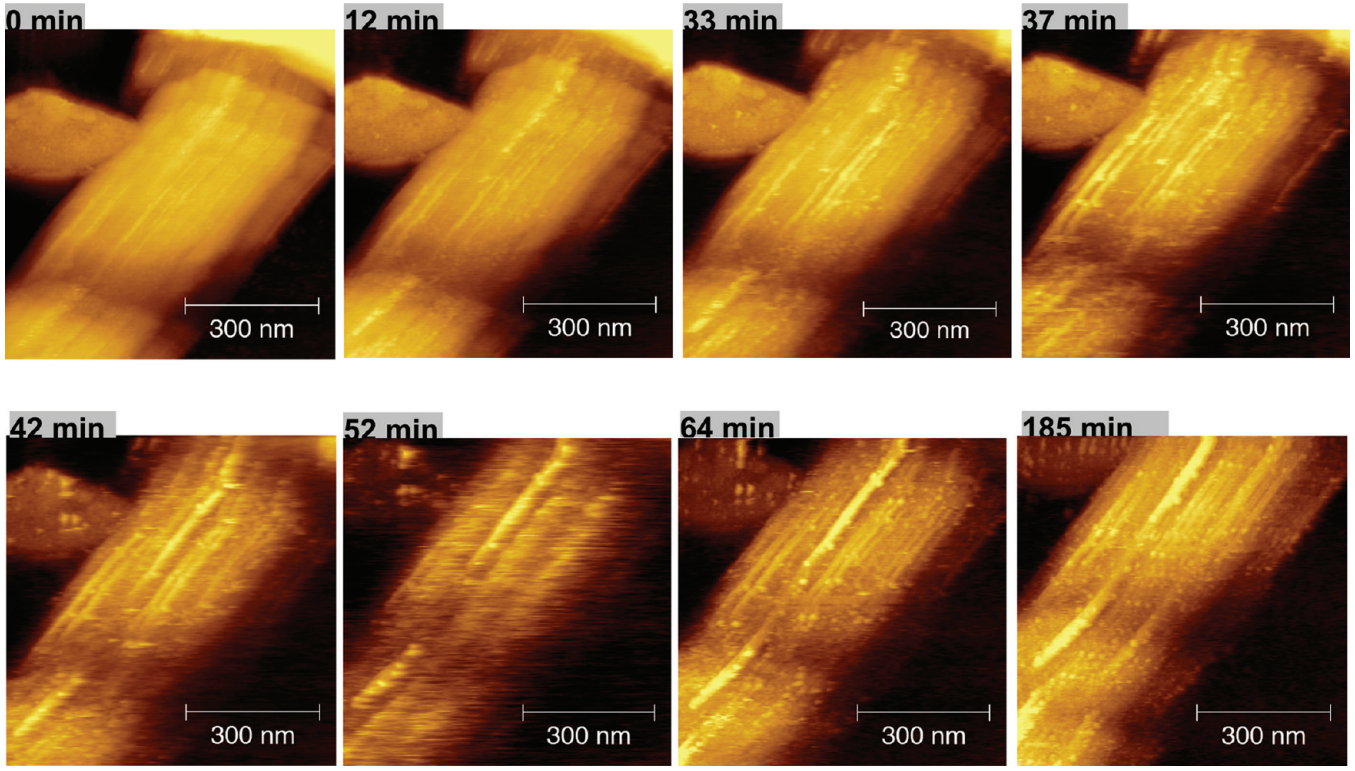

Figure 4. Changes to a crystalline cellulose fiber treated with Cel7B as monitored by real-time AFM. The fiber was incubated with 4 μg/mL Cel7B at pH 5.0, and AFM topography images of the same region were recorded at the times indicated. The color scales for all images were normalized individually to provide the proper contrast.

topography images. Complementary amplitude and phase images that were used to assist in the interpretation of the topography images are presented in the Supporting Information.

The high-resolution topography image of a single fiber recorded in buffer before the addition of enzyme is shown in Figure 3a. The image reveals the hierarchical structure of the fiber that consists of many tightly packed microfibrils. The cross-sectional profile presented in Figure 3b shows that surface corrugation due to the packing of microfibrils has a periodicity of approximately 4−6 nm, which was taken as a measure of the microfibril width. A histogram of the microfibril widths constructed from many cross-sectional profiles is presented in Figure 3c. It reveals that the average width of the microfibril is 5 ± 2 nm. This result is in agreement with published data in which the width of microfibrils is reported to range from 4.4 to 7.9 nm, depending on the cellulose source and the pretreatment method.[32,34]

To ensure that prolonged AFM imaging did not cause a mechanical disruption or disintegration of the fibers, images of the same spot on a single fiber in buffer were collected over a period of 2 h without the addition of enzyme. In Figure SI-4 in the Supporting Information, we show selected AFM topography images obtained in this experiment. The morphology of the fiber remains unchanged throughout the imaging period. Variations of 4% in volume and less than 0.1 nm rms in surface roughness were calculated for selected fragments of the fiber from this control experiment. These values represent random errors and instrumental drift at prolonged scanning times.[19]

In Situ Real-Time AFM Imaging of Cellulose Degradation by Cel7B. Figure 4 shows a series of time-lapse topography images collected on the target fiber after the addition of 4 μg/mL Cel7B to the AFM cell. The image collected before exposure to enzyme shows that the selected target consists of a large fiber in the middle of the image and a small clump of fibers lying to the upper left. The position of the small clump was used as a marker to correct for the AFM piezo drifts during the long experiment and to analyze changes in the same fragment of the large fiber. After the acquisition of this image, the enzyme solution was added to the liquid cell. The seven additional images in Figure 4 were collected at different times during the 185 min experiment. The images show that the fiber becomes progressively more corrugated with time because of either erosion or the swelling of individual microfibrils. These changes with time can be seen very clearly in a movie included in the Supporting Information (Movie SI-1) that provides an animated illustration of the enzyme-induced changes in the fiber-surface topography. As complementary evidence, the corresponding amplitude and phase images are also provided in the Supporting Information (Figure SI-5).

Cross-sectional analysis was performed to quantify the topographical changes observed in Figure 4. Height profiles were selected and plotted (Figure 5) for a sampling line that runs across the large fiber, which is marked in the inset image. These profiles show that the average height of the fiber progressively decreases during the initial ∼50 min of incubation with the enzyme. It reaches a minimum at ∼50−60 min and then increases during the remaining course of the experiment until the final image collected at 185 min. The profile shows that the surface roughness of the fiber significantly increases with the incubation time. In addition, several peaks on the surface profile appear and disappear during the incubation. This activity is clearly visible in Movie SI-1 as blinking stripes corresponding to individual microfibrils that appear and disappear with time. In addition, it can be seen in Movie SI-1

dx.doi.org/10.1021/la301030f | *Langmuir* 2012, 28, 9664−9672

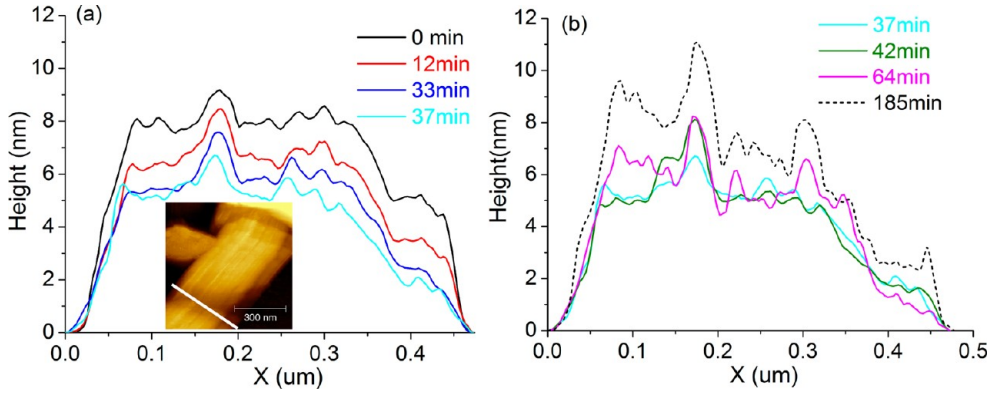

Figure 5. Changes in the height profile of a fiber during treatment with Cel7B (a) during the first 37 min and (b) during the 37−185 min period. The heights across the same section of a fiber (inset) were determined from AFM topography images of the same target at the times indicated. The cross-sectional line length and width were 475 and 25 nm, respectively.

that microfibrils are cleaved by the enzyme, thereby exposing new fibril ends. The cross-sectional analysis also shows that the changes in surface topography take place predominantly in the direction normal to the fiber surface. This may be explained by the fact that the area on top of the surface is about 20 to 50 times larger than the area on the side of the fiber. Enzymatic digestion and swelling are surface reactions proportional to the surface area.

To acquire statistically representative information and to quantify the swelling of fibers, the volume of a selected fragment and its surface rms roughness were calculated and plotted as a function of the incubation time (Figure 6). The volumes were

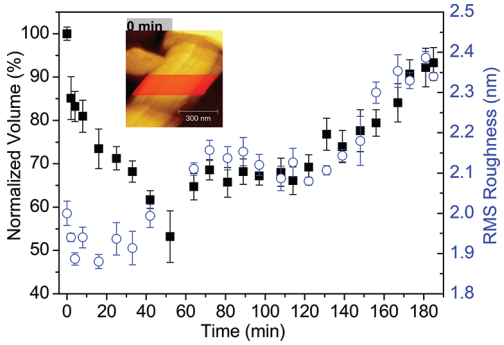

Figure 6. Changes in volume and surface rms roughness of a fiber with Cel7B treatment. The fiber volumes (i.e., $V_{time}/V_{0\ min} \times 100\%$) and surface rms roughness were calculated on the basis of the bulk fiber region denoted by the red mask in the inset image.

normalized with respect to the initial volume of the fiber, and they are plotted as a percentage of the volume measured before introducing the enzyme (zero-time volume). The volume decreased steadily during the first 50−60 min, reaching a minimum value of approximately 60%, which indicates that an active hydrolysis event has led to the loss of fiber volume and consequently mass. The volume remained almost constant during the next 60 min, and then it began to increase, reaching 93% of its initial value after 185 min. This distinctive time dependence of the volume was accompanied by a progressive increase in the rms roughness by about 0.5 nm. The volume changes that can be observed in Figure 6 are significantly greater than the random variations in volume and rms roughness of the surface observed in the control experiments. Therefore, the observed changes are the result of the action or presence of Cel7B on the fiber. A second example of these enzyme-induced changes to the volume and rms surface roughness of another fiber fragment is presented in Figure SI-6 of the Supporting Information, and the results of these analyses agree well with the data presented in Figure 6. Further analyses were performed on several other single cellulose fibers, yielding similar results (data shown in Figures SI-7 and SI-8 of the Supporting Information). These observed changes thus indicate the direct effect of Cel7B on a cellulose fiber. It seems that hydrolysis dominates the early stages of the enzyme−fiber interaction, followed by swelling, which suggests that a catalytically active enzyme is required for both effects. An analysis of approximately 300 swollen microfibrils following the Cel7B treatment revealed that their average width had doubled to 10 ± 4 nm (Figure 7). This

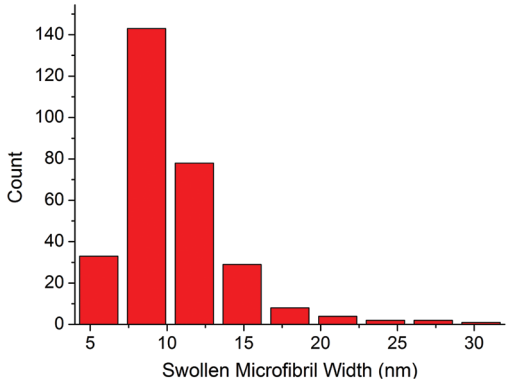

Figure 7. Distribution of widths of 300 swollen microfibrils (average width = 10 ± 4 nm).

number may suggest that the imaged features correspond to either a swollen single microfibril or two microfibrils stacked together.

To confirm that the swelling of a cellulose fiber requires its initial hydrolysis by Cel7B and does not result from the simple binding of the enzyme, the experiments described above were repeated with the isolated CBM of Cel7B. These time-resolved AFM experiments were performed using the recombinant GFP-CBM fusion protein at concentrations comparable to that of Cel7B (viz. ≤5.1 μg/mL). Under these conditions, GFP-CBM alone without the catalytic domain did not cause any hydrolysis, as expected, nor did it cause any discernible changes to the fiber morphology (Figure SI-9 of the Supporting Information). However, some swelling of the fibers was observed after CBM

dx.doi.org/10.1021/la301030f | Langmuir 2012, 28, 9664−9672

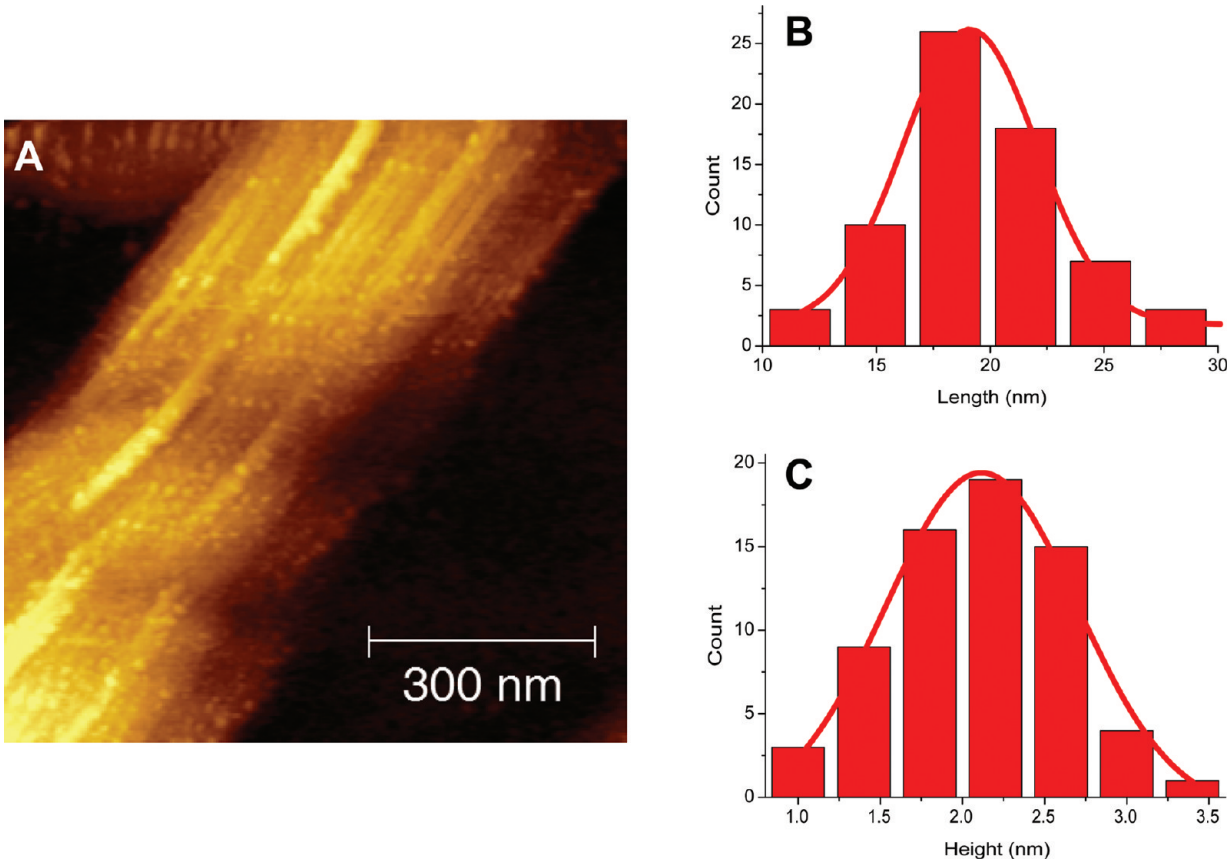

Figure 8. Detection of immobilized Cel7B on the surface of a microfibril after prolonged incubation. (A) AFM topography image of a fiber after 185 min of incubation with 4 μg/mL Cel7B (the same image as presented in Figure 4). Distributions of (B) length and (C) height of the putative enzyme molecules.

was introduced at concentrations greater than 7 μg/mL, a result that is consistent with a report that CBM plays a role in disrupting the hydrogen-bonding system of cellulose microfibrils.[10]

Our AFM data presented above are in good agreement with those obtained by Josefsson et al.[33] in QCM-D studies of cellulose films incubated with Cel7B. These films were spin coated from *N*-methylmorpholine-*N*-oxide (NMMO) and contained a significant portion of the cellulose II structure. The QCM-D signal frequency decreased during incubation with the enzyme and reached a plateau as a function of time. The decrease in frequency indicated an increase in the mass and was interpreted as the swelling of cellulose fibers. Our results, however, provide further important insight into the mechanism of swelling of native crystalline cellulose by showing that it involves the loosening of the fiber structure and the exposure of individual microfibrils. These results may be explained in the context of models of microfibril assembly that have been proposed for plant[12] and bacterial cellulose.[29,34] These models assume that individual microfibrils consist of parallel glucan chains that pack within the interior and are surrounded by noncrystalline or para-crystalline chains distributed in the outer sheath of the microfibril that serves as a gluelike component that chemically holds the crystalline chains together. It has been proposed that Cel7B is capable of preferentially hydrolyzing amorphous cellulose while being virtually nonactive on crystalline cellulose.[5,22] Therefore, the action of Cel7B would result in the introduction of water into the exposed hydrophilic structure of the inner para-crystalline cellulose chains, thereby triggering the observed swelling of microfibrils. This swelling event would be a relatively slow process as water molecules penetrate the space between adjacent cellulose chains, causing a rebalancing of the intermolecular hydrogen-bonding network and resulting in the dilation of the physical dimensions of the microfibrils. Such swelling would thus occur predominantly after the degradation of the surface protective layers of cellulose chains as catalyzed by Cel7B. By exposing the cellulose only to isolated CBM, we observed no significant swelling that indicated that active hydrolysis is required for swelling to occur.

Many of the images of cellulose microfibrils treated with Cel7B revealed the presence of small bright spots, with the number of these bright spots increasing with incubation time. On the basis of the reports of Lee et al.[33] and Igarashi et al.,[17,18] it is likely that these bright spots correspond to individual enzymes that are bound to the surface of the cellulose. Such an image is shown in Figure 8a following the incubation of a microfibril with the enzyme for 185 min. An analysis of this and similar images indicated that the average length (Figure 8b) and height (Figure 8c) of these bright spots were 19 $\pm$ 4 and 2.2 $\pm$ 0.5 nm, respectively. These values are consistent with small-angle X-ray scattering data that showed that Cel7B has a "tadpole" shape with an overall length of 18 nm and a diameter of 5.3 nm.[36] Although the length of the enzyme is in excellent agreement with the average length of the observed bright spots, the height of the bright spots is less than the diameter that has been reported for the enzyme. However, Igarashi et al.[17] have also observed by high-speed AFM that the height of *T. reesei*

dx.doi.org/10.1021/la301030f | *Langmuir* 2012, 28, 9664−9672

CBHI on a cellulose fiber was underestimated (a measured value of 3.1 nm compared to the value of 4.5 nm determined using small-angle X-ray scattering[37]). It is quite likely that the enzymes are compressed by the AFM tip during image acquisition so that the measured vertical dimension is reduced from its actual value.

SUMMARY AND CONCLUSIONS

We employed an in situ AFM imaging technique to visualize the action of *T. reesei* Cel7B directly on a single BC fiber. The fiber volume and its surface roughness were calculated from the AFM images. Increases in the fiber surface roughness and decreases in the fiber volume were the direct result of Cel7B action on the fiber. Changes in these parameters with time showed that Cel7B's activity initially involves hydrolysis and then swelling. The high-resolution AFM images revealed that the combined action of these two processes results in loosening of the fiber structure that exposes single microfibrils or bundles of microfibrils on the fiber surface. Our observations confirm that Cel7B preferentially digests amorphous or para-crystalline fragments of the fiber, thereby exposing the crystalline microfibrils. These direct observations thus serve to explain the synergistic effect of Cel7B with Cel7A and Cel6A enzymes.[5] Our results clearly show that Cel7B exposes crystalline microfibrils and creates microfibril ends and in this way assists the two cellobiohydrolases in digesting these microfibrils. We anticipate that the application of our AFM-based analysis to other cellulolytic enzymes, alone and in combination, will provide significant insight into the process of cellulose biodegradation and greatly facilitate its application to the efficient and economical production of cellulosic ethanol.

ASSOCIATED CONTENT

Supporting Information

Evaluation of enzyme purity by the SDS-PAGE method. Calibration curve of a reducing sugar assay and the assay results for additional samples. Topography images and data analysis for control experiments performed in the absence of Cel7B. Topography images obtained in situ on bacterial cellulose fibers incubated in aqueous solutions of GFP-CBM. Corresponding amplitude and phase images recorded on the target fiber. Data analysis for a different fragment of the target fiber. Real-time AFM images and analyses of the fiber volume change obtained from two additional trials with Cel7B = 7.6 μg/mL. A movie consisting of a series of time-lapse AFM topography images. This material is available free of charge via the Internet at http://pubs.acs.org.

AUTHOR INFORMATION

Corresponding Author

*E-mail: jlipkows@uoguelph.ca.

Notes

The authors declare no competing financial interest.

ACKNOWLEDGMENTS

We thank Chris Vandenende for his technical assistance with the preparation of bacterial cellulose. This work has been supported by a collaborative research and development grant from the Natural Sciences and Engineering Research Council of Canada (CRDPJ401727-10) to J.L., J.R.D., and A.J.C. J.R.D. and J.L. also acknowledge Canada Research Chair awards.

REFERENCES

(1) Clarke, A. J. *Biodegradation of Cellulose: Enzymology and Biotechnology*; CRC Press: Boca Raton, FL, 1997.
(2) Klemm, D.; Heublein, B.; Fink, H.-P.; Bohn, A. Cellulose Fascinating Biopolymer and Sustainable Raw Material. *Angew. Chem., Int. Ed.* **2005**, *44*, 3358−3393.
(3) Nishiyama, Y.; Langan, P.; Chanzy, H. Crystal Structure and Hydrogen-Bonding System in Cellulose Iβ from Synchrotron X-ray and Neutron Fiber Diffraction. *J. Am. Chem. Soc.* **2002**, *124*, 9074−9082.
(4) Nishiyama, Y.; Sugiyama, J.; Chanzy, H.; Langan, P. Crystal Structure and Hydrogen Bonding System in Cellulose Iα from Synchrotron X-ray and Neutron Fiber Diffraction. *J. Am. Chem. Soc.* **2003**, *125*, 14300−14306.
(5) Zhang, Y. H. P.; Lynd, L. R. Toward an Aggregated Understanding of Enzymatic Hydrolysis of Cellulose Noncomplexed Cellulase Systems. *Biotechnol. Bioeng.* **2004**, *88*, 797−824.
(6) Wyman, C. E. What Is (and Is Not) Vital to Advancing Cellulosic Ethanol. *Trends Biotechnol.* **2007**, *25*, 153−157.
(7) Lynd, L. R.; Laser, M. S.; Bransby, D.; Dale, B. E.; Davison, B.; Hamilton, R.; Himmel, M.; Keller, M.; McMillan, J. D.; Sheehan, J.; Wyman, C. E. How Biotech Can Transform Biofuels. *Nat. Biotechnol.* **2008**, *26*, 169−172.
(8) Mansfield, S. D.; Mooney, C.; Saddler, J. N. Substrate and Enzyme Characteristics that Limit Cellulose Hydrolysis. *Biotechnol. Prog.* **1999**, *15*, 804−816.
(9) Eriksson, T.; Karlsson, J.; Tjerneld, F. A Model Explaining Declining Rate in Hydrolysis of Lignocellulose Substrates with Cellobiohydrolase I Cel7A and Endoglucanase I Cel7B. *Appl. Biochem. Biotechnol.* **2002**, *101*, 41−60.
(10) Arantes, V.; Saddler, J. N. Access to Cellulose Limits the Efficiency of Enzymatic Hydrolysis the Role of Amorphogenesis. *Biotechnol. Biofuels* **2010**, *3*, 4.
(11) Hall, M.; Bansal, P.; Lee, J. H.; Realff, M. J.; Bommarius, A. S. Cellulose Crystallinity—A Key Predictor of the Enzymatic Hydrolysis Rate. *FEBS J.* **2010**, *277*, 1571−1582.
(12) Ding, S.-Y.; Himmel, M. E. The Maize Primary Cell Wall Microfibril A New Model Derived from Direct Visualization. *J. Agric. Food Chem.* **2006**, *54*, 597−606.
(13) Bastidas, J. C.; Venditti, R.; Pawlak, J.; Gilbert, R.; Zauscher, S.; Kadla, J. F. Chemical Force Microscopy of Cellulosic Fibers. *Carbohydr. Polym.* **2005**, *62*, 369−378.
(14) Baker, A. A.; Helbert, W.; Sugiyama, J.; Miles, M. J. High-Resolution Atomic Force Microscopy of Native Valonia Cellulose I Microcrystals. *J. Struct. Biol.* **1997**, *119*, 129−138.
(15) Santa-Maria, M.; Jeoh, T. Molecular-Scale Investigations of Cellulose Microstructure during Enzymatic Hydrolysis. *Biomacromolecules* **2010**, *11*, 2000−2007.
(16) Liu, Y.-S.; Baker, J. O.; Zeng, Y.; Himmel, M. E.; Haas, T.; Ding, S.-Y. Single Molecule Study of Cellulase Hydrolysis of Crystalline Cellulose. *J. Biol. Chem.* **2011**, *286*, 11195−11201.
(17) Igarashi, K.; Koivula, A.; Wada, M.; Kimura, S.; Penttilä, M.; Samejima, M. High Speed Atomic Force Microscopy Visualizes Processive Movement of Trichoderma reesei Cellobiohydrolase I on Crystalline Cellulose. *J. Biol. Chem.* **2009**, *284*, 36186−36190.
(18) Igarashi, K.; Uchihashi, T.; Koivula, A.; Wada, M.; Kimura, S.; Okamoto, T.; Penttilä, M.; Ando, T.; Samejima, M. Traffic Jams Reduce Hydrolytic Efficiency of Cellulase on Cellulose Surface. *Science* **2011**, *333*, 1279−1282.
(19) Quirk, A.; Lipkowski, J.; Vandenende, C.; Cockburn, D.; Clarke, A. J.; Dutcher, J. R.; Roscoe, S. G. Direct Visualization of the Enzymatic Digestion of a Single Fiber of Native Cellulose in an Aqueous Environment by Atomic Force Microscopy. *Langmuir* **2010**, *26*, 5007−5013.
(20) Kleywegt, G. J.; Zou, J.-Y.; Divne, C.; Davies, G. J.; Sinning, I.; Stahlberg, J.; Reinikainen, T.; Srisodsuk, M.; Teeri, T. T.; Jones, T. A. The Crystal Structure of the Catalytic Core Domain of Endoglucanase I from Trichoderma reesei at 3.6 Å Resolution, and a Comparison with Related Enzymes. *J. Mol. Biol.* **1997**, *272*, 383−397.

(21) Nakazawa, H.; Okada, K.; Kobayashi, R.; Kubota, T.; Onodera, T.; Ochiai, N.; Omata, N.; Ogasawara, W.; Okada, H.; Morikawa, Y. Characterization of the Catalytic Domains of Trichoderma reesei Endoglucanase I, II, and III, Expressed in Escherichia coli. *Appl. Microbiol. Biotechnol.* **2008**, *81*, 681−689.
(22) Lynd, L. R.; Weimer, P. J.; van Zyl, W. H.; Pretorius, I. S. Microbial Cellulose Utilization Fundamentals and Biotechnology. *Microbiol. Mol. Biol. Rev.* **2002**, *66*, 506−577.
(23) Delmer, D. P. Cellulose Biosynthesis: Exciting Times for A Difficult Field of Study. *Annu. Rev. Plant Physiol.* **1999**, *50*, 245−276.
(24) Bhikhabhai, R.; Johansson, G.; Pettersson, G. Isolation of Cellulolytic Enzymes from Trichoderma reesei QM 9414. *J. Appl. Biochem.* **1984**, *6*, 336−345.
(25) Bradford, M. M. A Rapid and Sensitive Method for the Quantitation of Microgram Quantities of Protein Utilizing the Principle of Protein-Dye Binding. *Anal. Biochem.* **1976**, *72*, 248−254.
(26) Laemmli, U. K. Cleavage of Structural Proteins during the Assembly of the Head of Bacteriophage T4. *Nature* **1970**, *227*, 680−685.
(27) Birkett, C. R.; Foster, K. E.; Johnson, L.; Gull, K. Use of Monoclonal Antibodies to Analyse the Expression of a Multi-Tublin Family. *FEBS Lett.* **1985**, *187*, 211−218.
(28) Nie, H.-Y.; Walzak, M. J.; McIntyre, N. S. Use of Biaxially-Oriented Polypropylene Film for Evaluating and Cleaning Contaminated Atomic Force Microscopy Probe Tips: An Application to Blind Tip Reconstruction. *Rev. Sci. Instrum.* **2002**, *73*, 3831−3836.
(29) Astley, O. M.; Chanliaud, E.; Donald, A. M.; Gidley, M. J. Structure of *Acetobacter* Cellulose Composites in the Hydrated State. *Int. J. Biol. Macromol.* **2001**, *29*, 193−202.
(30) Ge, G.; Han, D.; Lin, D.; Chu, W.; Sun, Y.; Jiang, L.; Ma, W.; Wang, C. MAC Mode Atomic Force Microscopy Studies of Living Samples, Ranging from Cells to Fresh Tissue. *Ultramicroscopy* **2007**, *107*, 299−307.
(31) Sitterberg, J.; Ozcetin, A.; Ehrhardt, C.; Bakowsky, U. Utilising Atomic Force Microscopy for the Characterisation of Nanoscale Drug Delivery Systems. *Eur. J. Pharm. Biopharm.* **2010**, *74*, 2−13.
(32) Yarbrough, J. M.; Himmel, M. E.; Ding, S.-Y. Plant Cell Wall Characterization Using Scanning Probe Microscopy Techniques. *Biotechnol. Biofuels* **2009**, *2*, 17.
(33) Josefsson, P.; Henriksson, G.; Wagberg, L. The Physical Action of Cellulases Revealed by a Quartz Crystal Microbalance Study Using Ultrathin Cellulose Films and Pure Cellulases. *Biomacromolecules* **2008**, *9*, 249−254.
(34) Tischer, P. C. S. F.; Sierakowski, M. R.; Westfahl, H., Jr.; Tischer, C. A. Nanostructural Reorganization of Bacterial Cellulose by Ultrasonic Treatment. *Biomacromolecules* **2010**, *11*, 1217−1224.
(35) Lee, I.; Evans, B. R.; Woodward, J. The Mechanism of Cellulase Action on Cotton ″Bers—Evidence from Atomic Force Microscopy. *Ultramicroscopy* **2000**, *82*, 213−221.
(36) Abuja, P. M.; Hayn, M.; Chen, H.; Esterbauer, H. The Structure of Endoglucanase I (Trichoderma reesei) in Solution. *Prog. Colloid Polym. Sci.* **1993**, *93*, 181.
(37) Abuja, P. M.; Schmuck, M.; Pilz, I.; Tomme, P.; Claeyssens, M.; Esterbauer, H. Structural and Functional Domains of Cellobiohydrolase I from Trichoderma reesei. *Eur. Biophys. J.* **1988**, *15*, 339−342.